Switched Reluctance Motor-based EV Drive with Bidirectional Grid Interaction

Aman Keshari[1], Dogga Raveendhra[1], BL Narasimha Raju[2], Pradyumn Chaturvedi[3], U Ramanjaneya Reddy[4]& Phaneendra Babu Bobba[5]
[1] EED, MNNIT Allahabad, [2] EED, NIT Warangal, [3]EED, VNIT Nagpur,[3]EEE Department, SRM AP, [5]EEE Department, GRIET Hyderabad

2024 IEEE 4th International Conference on Sustainable Energy and Future Electric Transportation (SEFET) | 979-8-3503-8399-7/24/$31.00 ©2024 IEEE | DOI: 10.1109/SEFET61574.2024.10717965

***Abstract*— This manuscript presents a novel Multi-function Switched Reluctance Motor (SRM) based Electric Vehicle (EV) Drive system with integrated Grid-to-Vehicle (G2V) & Vehicle-to-Grid/ Vehicle-to-Load (V2G/V2L) functionalities. The study focuses on the development of a Hybrid Energy Storage System (HESS) that combines the advantages of batteries and super-capacitors to enhance the overall performance and efficiency of EVs. The work begins by discussing the design and integration of the SRM drive system, highlighting its ability to provide multi-functionality while maintaining high levels of efficiency and reliability. The integration of G2V and V2G/V2L functions further enhances the flexibility and usability of the system, allowing for bidirectional power flow between the vehicle and the grid or other loads. One of the key contributions of this work is the development of a comprehensive model for the HESS, which takes into account the characteristics of both the battery and super-capacitor components. This model serves as a universal framework for evaluating different HESS configurations and optimizing their performance based on specific application requirements. The paper also discusses the extensive testing and analysis conducted to validate the proposed HESS system. Results demonstrate the high degree of efficiency achieved by the system, leading to extended battery life and improved overall energy management in EVs. Moreover, the HESS model proves to be versatile, offering insights into power characteristics and aiding in the customization of battery configurations and controller settings.**

Keywords—EV, HESS, G2V

I. INTRODUCTION

Electric Vehicles (EV) plays a vital role in decreasing the dependency on fossil fuels, which leads to eco-friendly solution for smart mobility. Furthermore, EVs have various substantial benefits, such as lower global greenhouse gas (GHG) emissions and greater vehicle performance [1]. Onboard Chargers (OBCs) getting more popularity compared to off board charger as it can charge the vehicle at our convenience. Whereas off-board charger can charge only at fixed location. High power is limited by typical OBCs due to weight, size, and cost considerations. These problems can be resolved by integrating OBCs with the electric drive. Conductive or inductive on-board charging solutions are available. The connector and the charge inlet make direct contact when using conductive charging systems. Power is transmitted magnetically by an inductive charger [2].

With a bidirectional system that includes a BLIL boost converter and buck-boost converter, the electric-drive-reconstructed On-Board Charger (EDROC) can charge the battery pack while supporting power stability, battery energy injection back into the grid, and grid charging. The bidirectional EDROC allows for flexible V2G/V2L operating in the discharging mode, delivering high current output capabilities within the motor winding's safe limit. Bidirectional OBCs can return electrical energy to the grid, enabling vehicle-to-grid (V2G) capabilities that may be useful during periods of high power demand. Bidirectional OBCs would also allow EV owners to use their vehicles for other purposes, like vehicle-to-vehicle (V2V) operations in an emergency and vehicle-to-load (V2L) or vehicle-to-home (V2H) electricity in the event of a grid collapse [3].

Switch Reluctance Motor (SRM) lacks a permanent magnet and winding on its rotor as compared to PMSM. Therefore, the machine weighs less than a PMSM.SRM drives are emerging as a viable option for powertrains because of their many benefits, including excellent environmental adaptability, wide speed range, high starting torque, and lack of rare earth elements. When the motor is operating, the SRM system uses typical switch modules to excite the bipolar current and provide regenerative braking. These switch modules are mass-produced SRM drives for electric vehicles (EVs) with a balanced heat dissipation design. The proposed on-board charger integrates a front-end buck dc-dc converter and an EV switching reluctance motor (SRM) power converter to support several operation modes, including battery charging, regenerative braking, and vehicle running. Using the current power devices and SRM phase windings, OBC constructs a bridgeless ac-dc rectifier with power factor correction (PFC) capability for battery charging from the AC grid. Since the bridgeless rectifier uses the windings of two adjacent phases as energy-storage inductors, no extra power devices are needed for the battery-charging mode [4].

Power Factor Correction(PFC) can be divided into three parts namely a) Passive, b) Traditional(Boost, buck-boost, and Cuk based active PFC), c) Bridgeless Converter. The BLIL boost converter is used for power factor correction due to low switching loss and high power factor. In many different applications, including solar photovoltaic (PV) charging and plug-in electrical vehicle (PEV) charging, it is widely employed. A BLIL boost converter, buck-boost converter, or interleaved boost converter can replace the standard three-phase asymmetrical half-bridge (AHB) converter on the SRM drive to perform the charging function. It allows driving mode, vehicle-to-grid (V2G) charging mode, and solar PV charging mode without having an impact on the SRM's functionality. PV charging efficiency is enhanced by the interleaved boost converter, while the AC grid's power factor and power quality are enhanced by the PFC function [5]. The EDROC system reduces the need for additional charging units by utilizing the motor winding and propulsion inverter as the grid-side filter inductor and rectifier, respectively, makes the grid-to-vehicle (G2V) and vehicle-to-grid (V2G) charging modes viable. Additionally, it enables variable energy transmission between the battery pack, the AC grid, photovoltaic(PV) panels, and the SRM. Based on the quantity of converters, the charger can function independently in either driving or charging mode. It is categorized into three types: single-stage, double-stage, and composite converter systems. Without the need for further AC equipment, the suggested charger can be linked to the power grid via the power socket at home or in the workplace.

The double-stage converter system has more parts than the single-stage converter system and is typically used for three-phase fast charging. The proposed EDROC has a good suppression influence on the input current ripple and lowers current ripple by using an interleaving control technique. In the charging mode, it can reach unity power factor; in the

driving mode, it can discharge to power the motor. It is able to achieve a lower total harmonic distortion (THD) while simplifying the structure of existing EDROC without requiring additional equipment or specially created motors.

In order to improve the charging flexibility and cruising range of electric cars (EVs), raise the sustainability of the vehicle's operation and decrease dependency on the AC grid solar power is integrated into the electric drive rebuilt on-board charger (EDROC) system. The integration of solar power allows for the realization of vehicle-to-grid (V2G) and vehicle-to-load (V2L) functions, where excess energy generated by the PV panels can be fed back to the grid or used to power external loads. The integration of solar power aligns with the goal of achieving energy savings and emission reductions in the transportation sector. A highly integrated solution for electric vehicle (EV) applications, the PV-assisted bidirectional EDROC system combines solar photovoltaic (PV) panels with the electric drive reconstructed on-board charging (EDROC) system. Energy can be transferred between the battery pack, PV panels, AC grid, switched reluctance motor (SRM) drive, and PV panels in a flexible and effective manner with this technology. Benefits from this integrated system include increased flexibility in charging, increased range, and the possibility of energy savings and EV emission reductions.

The split-phase windings function as filters to achieve PFC and lower system losses by multiplexing them and reconstructing the converter topology. The windings are used to balance the switching losses and achieve bipolar current excitation, ensuring efficient operation and regenerative braking in the system. The windings also play a role in maintaining power balance and enabling flexible motoring, charging, and discharging functions in the system.

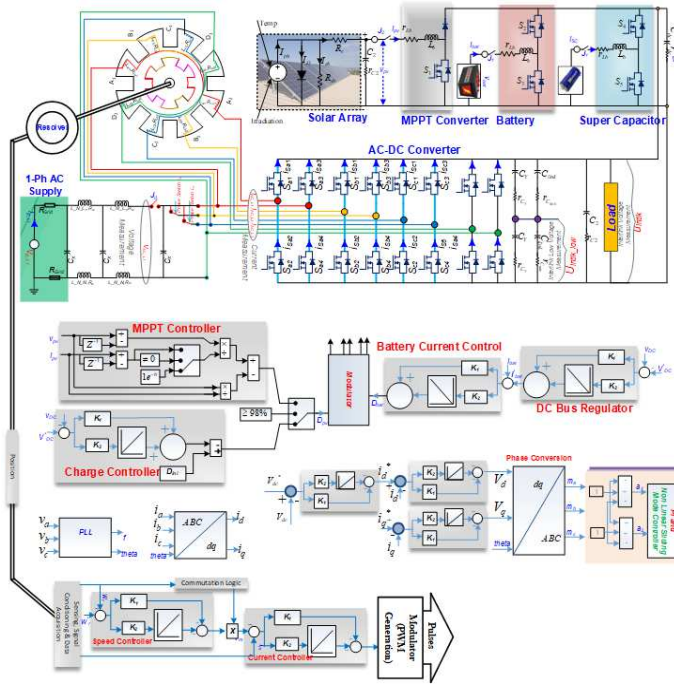

Fig. 1: Proposed Switched Reluctance Motor-based EV Drive with Bidirectional Grid Interaction.

The Proposed Switched Reluctance Motor based EV drive with bidirectional grid interaction is shown in Fig.1.The super-capacitor (SC) is the primary power source during vehicle start, while the battery provides power during runtime. These two components make up the energy storage system. Because of the SC's high power density, the starter can get enough current without degrading the battery's state of charge. Furthermore, the excess power can be used to recharge the battery from a low level of charge while the vehicle is operating. To connect the SC to a low-voltage battery, a DC-DC converter is utilized. When it comes to automotive applications, 48V and 10A battery packs with 13 series-2 parallel arranged lithium-ion batteries and a battery monitoring system (BMS) are the conventional design. The battery's level of charge must be tracked and managed by the BMS. However, because of their fast rate of discharge, super-capacitors are often avoided as energy storage devices even though they have an impressive power density.

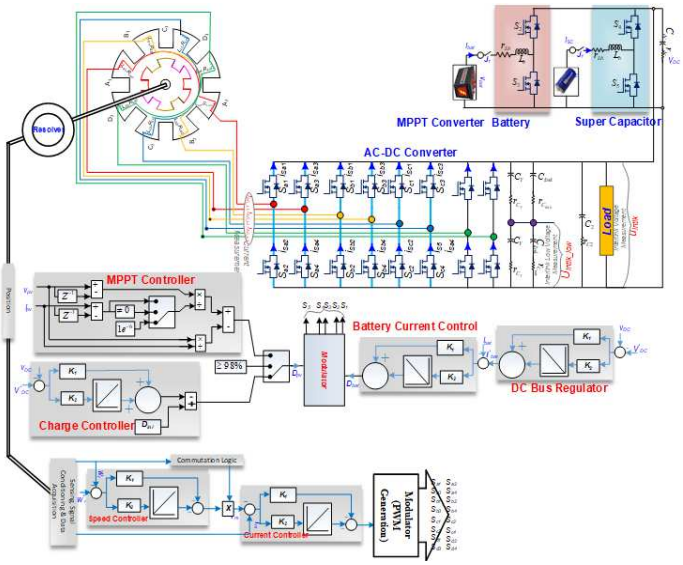

Fig. 2: Bipolar drive mode with switching states and phase current.

II. MOTORING MODE

A. Battery-to-Vehicle Driving State

Bipolar drive mode with switching states is shown in Fig.2. Bipolar control methods enhance dynamic dependability, reduce conduction loss, and dissipate heat for longer service lives. Each phase's current direction is changed when two distinct branches are conducted over consecutive electrical cycles. When Sa_2 and Sa_4 are ON, the phase winding in phase-A is electrified negatively; when Sa1 and Sa3 are ON, it is energized positively. To finish a full period, four consecutive electrical cycles are utilized, with the chopper switches in one phase operating sequentially.

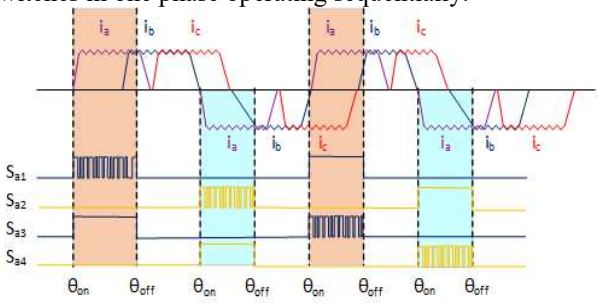

Fig. 3: Phase current during bipolar drive mode.

Phase current during bipolar drive mode is shown in Fig.3. Phase current are controlled and average output torque is increased by using several control methods, including Angle Position Control (APC), Voltage Chopping Control (VCC),

and Current Chopping Control (CCC). Figure 4(a) shows the CCC control system. To improve operational reliability and simplify control, a bipolar square-wave excitation form is used.

B. *Regenerative Braking State*

The SRM acts as a generator to stop overcurrent, and as Figure 4(b) illustrates, it is critical to measure the excitation current across the battery pack. Phase-A current is regulated by applying zero or negative phase voltage to account for the negative return electromotive force after it achieves its reference current. Next, the resulting negative torque is applied to the brakes.

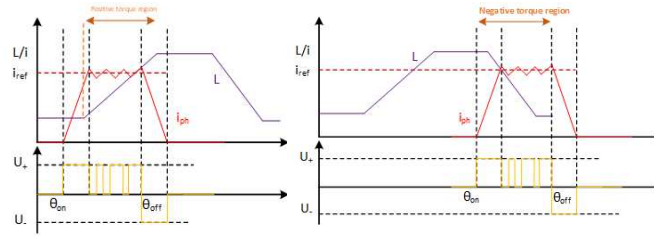

Fig. 4: Operational states. (a) Driving state. (b) Regenerative braking state.

III. BATTERY CHARGING MODES

A. *Charging States Analysis*

The proposed SRM system allows for flexible selection of the Super Capacitor and vehicle-roof PV panels are charge by battery pack without support of an external charger when it is operating in standstill mode.

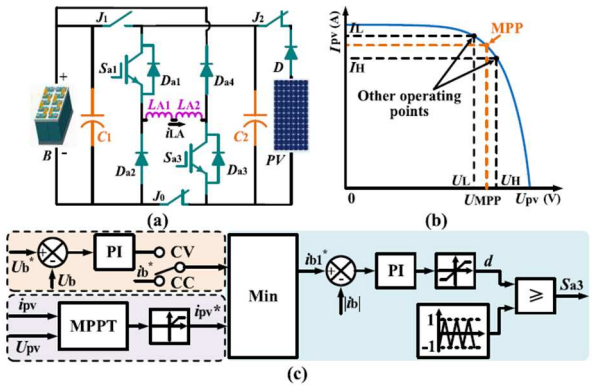

Fig.5: Operating Principle for PV-powered vehicle charging (a) Equivalent circuit. (b) Operating point (c) Control diagram.

PV panels charge battery packs with J0, J2 is ON and J1 is OFF, enabling zero-torque charging until Phase-A aligns with the SRM. The phase-A winding of a boost converter, as shown in Figure 5(a), is used for maximum power point tracking (MPPT) management. Current control can be used to establish the operating points depicted in Figure 5(b) to satisfy different charging demands.

U_{PV}: output voltage of the PV panels, I_{PV}: output current of the PV panels, U_{MPP}: output voltage of the PV panels operating at the maximum power point, I_L: lowest output current of the PV panels, U_L: lowest output voltage of the PV panels, I_H: highest output current of the PV panels, U_H: highest output voltage of the PV panels.

The battery pack can be charged using the rebuilt boost converter when it is in PV powered charging mode. By using an incremental conductance technique, PV panels can be configured to give the necessary output current for MPPT control.

B. *Single-Phase AC Grid Powered Charging State*

When J1 is on and J0 and J2 are off, the battery pack is charged using a power socket and a single-phase AC grid. An analogous circuit and control technique are shown in the diagram in Figure 6. The BLIL converter consists of two bridgeless boost converters connected in parallel that work alternately to prevent electromagnetic interference (EMI) from battery side conduction. It also includes an EMI filter. An inverter leg and phase-A winding rearranged creates a backend buck-boost circuit that may be used to charge a voltage or current continuously. Two boosted circuits are operated at equal duty ratios and with a half switching cycle delay in order to reduce harmonic elements, increase power factor, and raise the charging power level. The duty ratio (d) being more than or less than 0.5 influences the BLIL converter's operational characteristics.

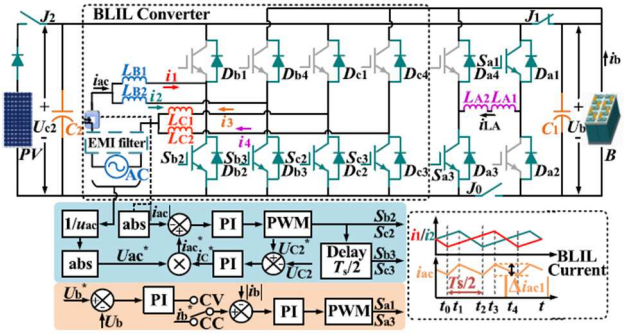

Fig. 6: Operation principle of single-phase ac powered charging.

C. Super Capacitor Powered Charging State

When the Hybrid Energy Storage System (HESS) is charging and the super-capacitor's State of Charge (SOC) exceeds the maximum bound indicated by $Q_{sc(charg)_{high}}$, the battery power limit is increased to $P_{charg\_high\_limit}$.Conversely, if the SOC of the super-capacitor falls below the lower limitation$Q_{sc(charg)_{low}}$, the limitation of battery power is reduced to $P_{charg\_low\_limit}$.

$$Q_{sc} - Q_{scref} \geqslant Q_{sc(charg)_{high}}$$
$$P_{batt_{charg_{lim}}} = P_{charg_{high_{lim}}}$$
$$Q_{sc} - Q_{scref} \geqslant Q_{sc(charg)_{low}}$$
$$P_{batt_{charg_{lim}}} = P_{charg_{high_{lim}}} \quad (1)$$

WhereQ_{sc}, Q_{scref}: charge of Supercapacitor

P_{batt}: Battery power lower and higher charge

D. *Torque Characteristics Under Charging Mode*

Due to the variation in the slope of the inductance curve with respect to position, the total torque is not always zero in the charging mode. In this study, fixed-point charging is used to achieve zero-torque functioning. Figure 8 illustrates the torque characteristic of the switched reluctance motor (SRM), which is zero total torque independent of phase-A current. In order to align the windings and produce equal phase inductances, phase-A is turned on first. L_{eq} is unaffected by magnetic saturations even at large input currents. Any three phases of the multiphase motor can be charged using the zero-torque charging approach.

E. Single-Phase AC Grid Powered Charging State

As per the approach depicted in Figure 6, the battery-less inductive link (BLIL) circuit's maximum branch current differential can be achieved at d = 0.5. This can be represented in the following manner:

$$\Delta i_{max} = \frac{U_{C_2} T_S}{4L_{B_1}} \quad (2)$$

During Charging process maximum torque is evaluated using the following presumption:

$$i_1 = i_2 + \Delta i_{max} \quad (3)$$

The highest value of the total torque during the single-phase AC grid's positive period can be found by:

$$T^P_{max} = T_A + T_B + T_C = \frac{K'}{4}\Delta i^2_{max} = \frac{1}{2}K\left(\frac{\Delta i_{max}}{2}\right)^2 \quad (4)$$

where the split and normal phase inductance's slope are denoted by K' and K, respectively where K' is half of K . Comparably, the maximum value of the single-phase AC grid's total instantaneous torque during its negative phase. The potential maximum torque of the electric vehicle (EV) during the charging process is significantly less than the static load when the charging phase current and slope factors differ by a tiny amount at a specific aligned location. In order to further reduce the instantaneous torque, the BLIL circuit's switching period can be limited using equation (3). Consequently, static charging can be carried out without the requirement for an extra clamping device.

F. PV Powered Charging

As phase-A inductance is the only one active for charging at the aligned state, its slope factor is zero. Because the instantaneous torque isn't zero, the rotor can stay in a stationary position.

IV. BATTERY DISCHARGING MODES

A. Equivalent Discharging Modes

1. V2G/V2L States Powered by Battery Pack:

Reconfigure the converter to produce a high current output capacity within the safe limit of current for the motor winding while keeping J0, J1, and J2 in the ON state when the needed voltage amplitude is less than that of the battery pack.

Two closed-loop control systems are used to supply power, either direct current or alternating current. For direct current loads, a unipolar double-frequency sinusoidal Pulse Width Modulation (PWM) technique is used for ac loads, a conventional chopper control mechanism is implemented. High levels of consistency can be seen in single-phase bridge circuits with parallel coupling and symmetric center split phase inductance.

As a result, the two parallel circuits' power switches that are positioned in the same way are controlled synchronously to regulate current sharing. When the required voltage amplitude exceeds the battery pack's capacity, the converter may need to be adjusted to maintain the relays J_0, J_1, and J_2 in the OFF position in order to provide high-voltage output capabilities. A double closed-loop control technique can be used to manage the cascaded single-phase bridge inverter, while constant voltage charging control can be used to control the output voltage of the buck-boost converter. The switches S_{b1} and S_{c2} remain in the ON position in tandem with the dc load's operation to prevent a reduction in operational efficiency caused by the two-stage dc conversion.

2. V2G/V2L States Powered by PV

To enable the vehicle to transition to the vehicle-to-grid or vehicle-to-load states, the photovoltaic panels can be used to deactivate J1 and activate J0 and J2 when there is sufficient solar radiation. The sequential converter depicted in Figure 11 is the result of combining a boost converter and a single-phase bridge converter. Primary power comes from photovoltaic panels, with power balance maintained by the battery pack. This single-phase bridge circuit again makes use of Maximum Power Point Tracking (MPPT) control, as shown in Figure 7.

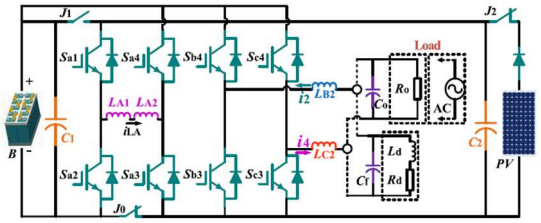

Fig. 7: PV-powered state of discharging

3. Super Capacitor Powered Charging State:

In the event that the super-capacitor's state of charge (SOC) exceeds the upper bound known as $Q_{sc(dischar)_{low}}$ during the HESS's discharge, the battery power limitation is raised to $P_{disch\_high\_limit}$.On the other hand, the battery power limitation is lowered to $P_{disch\_low\_limit}$. if the super-capacitor's SOC drops below the predefined lower limit known as $Q_{sc(dischar)_{low}}$,

$$Q_{sc} - Q_{scref} \geqslant Q_{sc(dischar)_{high}}$$
$$P_{batt_{charg_{lim}}} = P_{charg_{high_{lim}}}$$
$$Q_{sc} - Q_{scref} \geqslant Q_{sc(dischar)_{low}}$$
$$P_{batt_{charg_{lim}}} = P_{charg_{high_{lim}}} \quad (5)$$

B. Torque Characteristics under discharging Mode

Figure 8–10 makes it clear that there is no variation in the current flowing through the two BLIL branches over time. This means that throughout the discharge phase, the motor's total instantaneous torque is always zero, in accordance with the preset rotor orientation depicted in Figure 8.

(1) SRM Driving Operation

Using a common asymmetric half-bridge converter, the suggested integrated SRM drive's SRM driving function is depicted in Fig. 9. The commutation signals S_a, S_b, and S_c, as well as the position signals En_A, En_B, and En_Z, are feedback signals that produce the motor speed ω_r.

The commutation signals produce the G_A^-, G_B^-, and G_C^- gate signals.

$$G_A^- = S_a\,,\ G_B^- = S_b\ ,\ G_C^- = S_c \quad (6)$$

Three current commands i_a^*, i_b^*, i_c^* are synthesized by the current command generator

$$i_a^* = I_M^* \text{ x } S_a,\ i_b^* = I_M^* \text{ x } S_b,\ i_c^* = I_M^* \text{ x } S_c \quad (7)$$

Where the speed controller's output is the current command amplitude I_M^*.

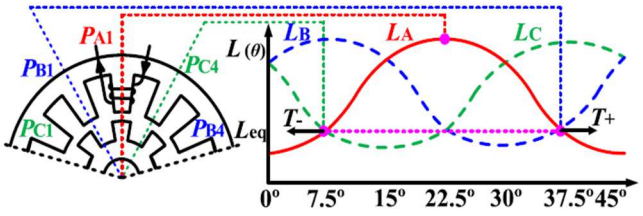

Fig. 8: Rotor position at standstill condition.

Three current controllers in Fig. 9 generate three control signals $V_{cont,a}$, $V_{cont,b}$ and $V_{cont,c}$, which are compared to the same triangular signal V_{tri} to produce three comparison signals d_a, d_b, and d_c. The gate signals are generated by the commutation signals and the comparison signals:

The commutation signals and comparison signals produce the gate signals G_A^+, G_B^+ and G_C^+.

$$G_A^+ = S_a \text{ x } d_a,\ G_B^- = S_b \text{ x } d_b,\ G_C^- = S_c \text{ x } d_c \quad (8)$$

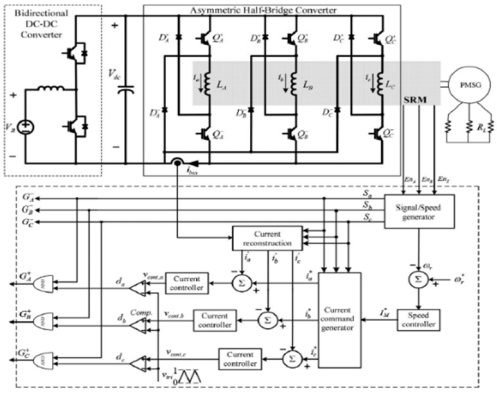

Fig.9: Operating mechanism of the suggested integrated SRM drive.

Switch bus current i_{bus} is detected by the physical current sensor in Figure 9. Fig. 3 shows a plot of all the current flowing routes for various gate signals. It can be observed that when both gate signals G_A^+ and G_A^- are low, current did not flow through the current sensor during the demagnetizing phase.. As a result, during current commutations, only magnetizing phase current is visible in the switch-bus current i_{bus}. Next, one can retrieve the phase currents that have been reconstructed by

$$i'_a = i_{bus} \text{ x } S_a$$
$$i'_b = i_{bus} \text{ x } S_b$$
$$i'_c = i_{bus} \text{ x } S_c \quad (9)$$

$$\text{signum}(x) = \begin{cases} -1, x < 0 \\ +1, x > 0 \end{cases} \quad (10)$$

$$v_{cont} = v_{PI} + v_{ff}^{G2V} \quad (11)$$

a) During Positive Half-Cycle ($V_s > 0$)

Positive grid current passes via the winding inductance L_A and the switch Q_A^- diode D_B^- when the signal G is high and the switch Q_A^- is conducting.

$$\begin{cases} i_{bus} = i_a = i_s \\ v_L = v_s > 0 \end{cases} \quad (12)$$

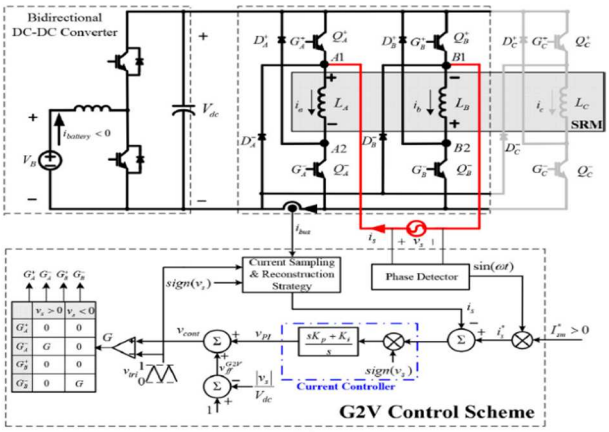

Fig. 10:Grid to Vehicle Charging

b) G2V Operation

Grid to vehicle operation is depicted in Fig.10. All switches are off when the signal G is low, and the winding inductance L_A, D_A^+,V_{dc} and D_B^--all experience positive grid current.

$$\begin{cases} i_{bus} = 0 \\ i_a = i_s \\ v_L = v_s - V_{dc} > 0 \end{cases} \quad (13)$$

$$< v_L >_{T_s} = v_s - (1 - v_{cont})V_{dc} \quad (14)$$

c) During Negative Half-Cycle ($v_s < 0$)

The diode $D_A^-$the switch bus, the switch $Q_B^-$and the winding inductance L_B all experience negative grid current when the signal G is high and the switch $Q_B^-$is conducting.

$$\begin{cases} i_{bus} = i_b = -i_s \\ v_L = v_s < 0 \end{cases} \quad (15)$$

All switches are off when the signal G is low, and the winding inductance L_B, D_A^-,V_{dc} and D_B^+ experience negative grid current flowing them.

$$\begin{cases} i_{bus} = 0 \\ i_b = -i_s \\ v_L = v_s + V_{dc} > 0 \end{cases} \quad (16)$$

$$< v_L >_{T_s} = v_s + (1 - v_{cont})V_{dc} \quad (17)$$

V. SYSTEM MODELLING

The average inductor voltage during the line cycle can be expressed by adding (14) and (17).

$$< v_L >_{T_s} = v_s - sign(v_s)(1 - v_{cont})V_{dc} \quad (18)$$

The feed forward term is determined by substituting (11) into (18) in order to remove the grid voltage disturbance impact.

$$v_{ff}^{G2V} = 1 - \frac{sign(v_s)v_s}{V_{dc}} = 1 - \frac{|v_s|}{V_{dc}} \quad (19)$$

From equation (18) average inductor voltage can be approximated as

$$< v_L >_{T_s} \approx sign(v_s)v_{PI}V_{dc} \quad (20)$$

As a result, the G2V current loop modeling becomes

$$\frac{i_s}{v_{PI}} = sign(v_s)\frac{V_{dc}}{sL+r} \quad (21)$$

Where L and r are winding inductance and resistance.

Table 1: Motor Specifications

Parameter	Value
Number of Phase	4
Stator Poles	8
Rotor Poles	6
Rated Torque	7 Nm
Rated Power	2.2 KW
Rated speed	3000 rpm
Resistance	0.7 Ω/ph

VI. SIMULATION RESULTS

The simulation validates the proposed multifunctional SRM system, which is based on a 8/6 SRM prototype with the primary parameters given in Table I. Because of the safe current limits on the motor winding, Level-1 charging power is taken into account.

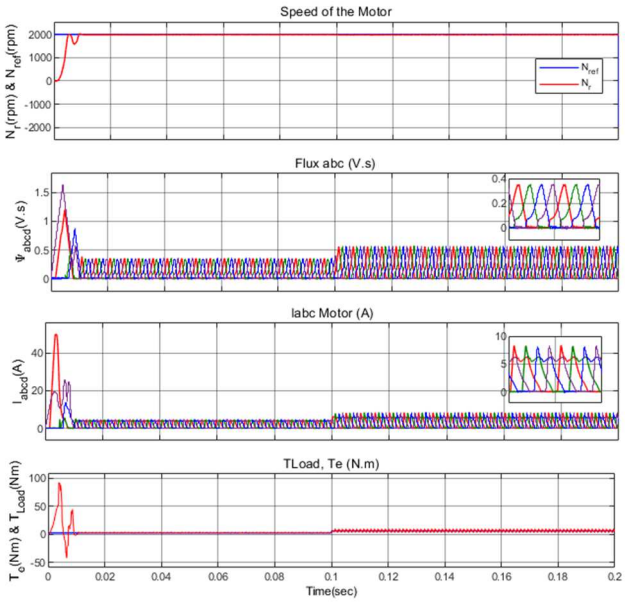

Fig. 11: Simulation Result under Motoring mode (a) Rotor speed, (b)Flux Linkage (c)Phase Current (d) Load Torque

As Depicted in Fig.11 under the motoring mode the speed of motor is constant at 2000 rpm and there is no fluctuations in speed waveform. The Flux Linkage and current waveform under this mode is depicted in Fig.11(b) and Fig.11(c) respectively. The Load Torque is changed at 0.1 sec and we get slight ripple after the introduction of changed torque. Moreover, for DC and single-phase AC discharging modes, output filter capacitor with ratings of 440μF/780V are introduced.

Table 2: Vehicle Roof PV Panel Parameters

Parameter	Value
U_{MPP}	30.3 V
I_{MPP}	8.27 A
P_{MPP}	250 W
U_{OC}	37.6 V
I_{SC}	8.85 A
K_i	0.0038537
K_v	-0.12032%

Only Phase A is excitation to aligned position prior to charging starting. It is evident that the battery voltage is around 400 V and the charging current is approximately 7.5 A during the charging process. A bidirectionally programmable direct current power supply simulates a 400-V/1000-Ah battery pack. The Voltage and current levels are being measured by Voltage measurement and Current measurement blocks in Simulink.

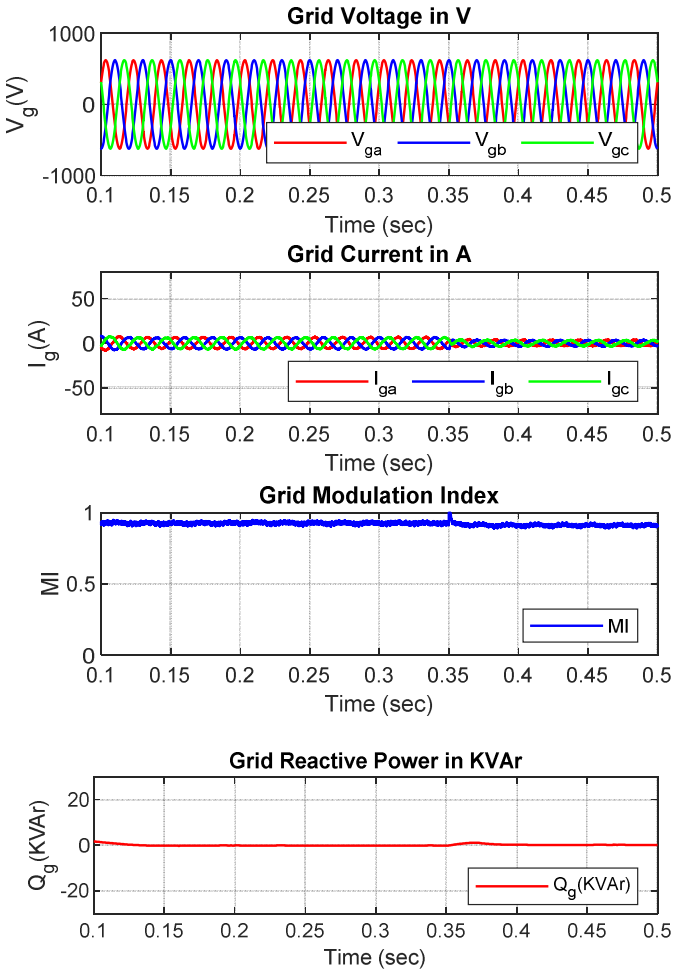

Fig. 12: Simulated results when charging with a single-phase ac grid. (a) Grid Voltage (b) Grid Current (c) Grid Modulation Index (d) Grid Reactive Power

Fig 12 represent the charging with the help of single phase ac grid where the grid voltage is depicted in Fig.12(a) where grid Voltage is 440V and grid current is shown Fig.12(b).Grid Modulation index is set to 0.9212 and its variation is shown in Fig.12(c).We can see in Fig.12(d) the reactive power is near to zero which means we are operating at unity power factor.

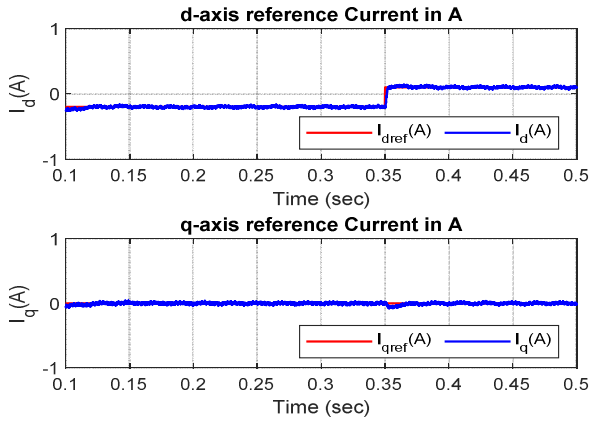

Fig 13: Waveform of current in d axis and q axis

The Parameters of PV used in the Simulation is listed in Table2.The maximum power of PV used is 250W. The Temperature coefficient of current is represented as K_i and Temperature Coefficient of Voltage is K_v. Source Transformation is applied and we are going to dq frame of reference. The current in d and q axis is shown in fig.13(a) and Fig.13(b).

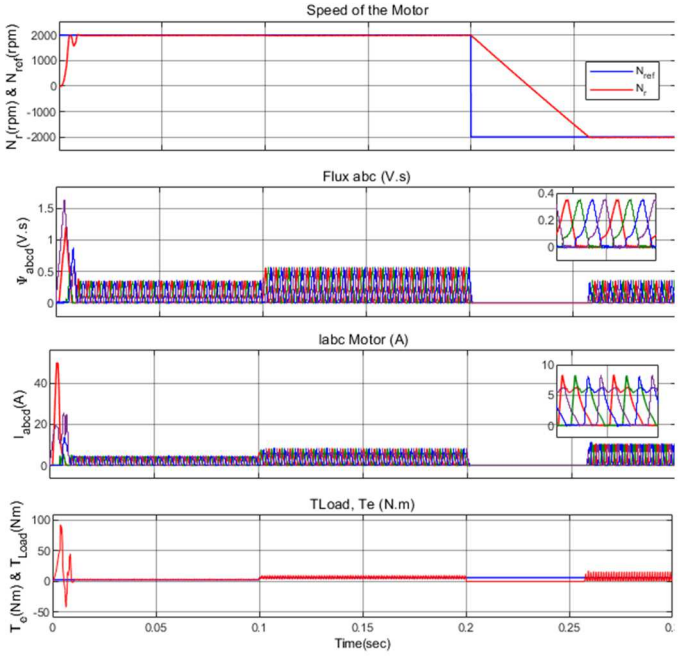

Fig. 8: Simulation Results under Regenerative Braking (a)Speed of Motor (b)Flux Linkage (c)Phase Current (d)Load Torque and Electromagnetic Torque

Fig. 14(a) and (b) show the simulation results in (a) we can see that motor goes into braking state as speed of motor comes down from 2000 rpm to -2000 rpm. The Flux Linkage and Current through the motor windings is shown in Fig.14(b) and Fig.14(c) respectively. We can also see in Fig.14(d) the load torque is constant when the motor goes into regenerative braking and it tends to be smooth as required.

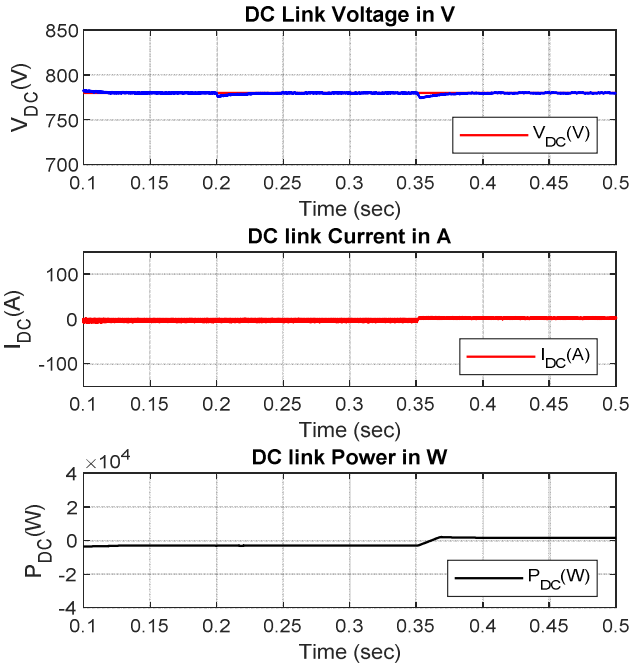

Fig 15. Results of DC Link

The DC Link various waveform listed in Fig.15.The Dc Link Voltage is constant instead of some disturbances as shown at 0.2 sec and 0.35 sec it tries to achieve constant Voltage as shown in Fig.15(a)The DC Link Current and Power Waveform is shown in Fig.15(b)and Fig.15(c) respectively.

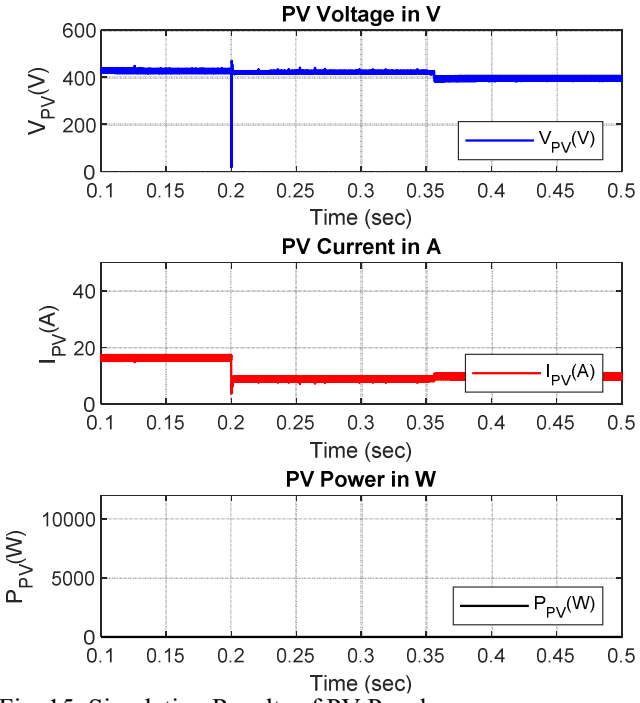

Fig. 15: Simulation Results of PV Panel

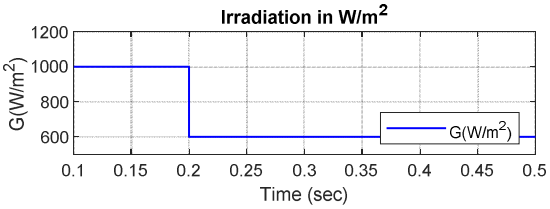

Fig 16. Solar irradiance variation

The Irradiance Waveform is Listed in Fig.16. The solar irradiance is intially at 1000W/m^2 and it comes down to 600W/m^2 in 0.25 seconds. The number of PV cells are 72 and PV array are arranged in a manner such that 14 are in series and one in a parallel.

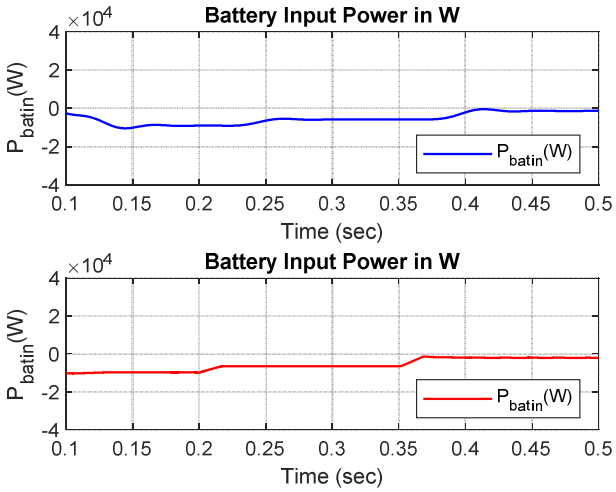

Fig.17 Power drawn/supplied from/to Battery

Fig. 17 represents the Power drawn from the battery. Variation in Input Power is shown in Fig.17(a) shows that power drawn is negative hence the battery is discharging and supplying power to the motor. There is a noticeable decrease in the amplitude of the output current as the load resistance increases. Discharging current rises to the values that fall inside the motor's safe limit. The system can be static discharged since the motor position can remain in its starting position in both dynamic and static discharging scenarios.

VII. CONCLUSION

The high degree of efficiency exhibited by the Hybrid Energy Storage System (HESS) created in this study helps to prolong the battery's life. This innovative system is tailored not only for application in HEVs and EVs but also serves as an effective energy storage solution for solar power. The model established in this research can serve as a universal framework for HESS systems, allowing for the evaluation of battery and super-capacitor attributes across various configurations. Given the extensive testing and analysis involved in battery pack design, the utilization of this model can offer a comprehensive system perspective while minimizing the need for such resource-intensive steps. Through customization of the battery configuration and fine-tuning of the controller based on this setup, the power characteristics can be accurately assessed, highlighting the distinct advantages of the proposed HESS.

VIII. REFERENCES

[1]. A. Khaligh and M. D'Antonio, "Global Trends in High-Power On-Board Chargers for Electric Vehicles," in IEEE Transactions on Vehicular Technology, vol. 68, no. 4, pp. 3306-3324, April 2019.

[2]. M. Yilmaz and P. T. Krein, "Review of Battery Charger Topologies, Charging Power Levels, and Infrastructure for Plug-In Electric and Hybrid Vehicles," in IEEE Transactions on Power Electronics, vol. 28, no. 5, pp. 2151-2169, May 2013.

[3]. J. Yuan, L. Dorn-Gomba, A. D. Callegaro, J. Reimers and A. Emadi, "A Review of Bidirectional On-Board Chargers for Electric Vehicles," in IEEE Access, vol. 9, pp. 51501-51518, 2021.

[4]. Q. Sun, H. Xie, X. Liu, F. Niu and C. Gan, "Multiport PV-Assisted Electric-Drive-Reconstructed Bidirectional Charger with G2V and V2G/V2L Functions for SRM Drive-Based EV Application," in IEEE Journal of Emerging and Selected Topics in Power Electronics, vol. 11, no. 3, pp. 3398-3408, June 2023.

[5]. J. Cai and X. Zhao, "An On-Board Charger Integrated Power Converter for EV Switched Reluctance Motor Drives," in IEEE Transactions on Industrial Electronics, vol. 68, no. 5, pp. 3683-3692, May 2021.

[6]. G. Subramanian and J. Peter, "Integrated Li-Ion Battery and Super Capacitor based Hybrid Energy Storage System for Electric Vehicles," 2020 IEEE International Conference on Electronics, Computing and Communication Technologies (CONECCT), Bangalore, India, 2020, pp. 1-6.

[7]. C. Feng, J. Wu, Q. Sun, H. Wu and L. Zhang, "An Integrated BLIL Boost Converter-based Switched Reluctance Motor Drive for PEV Applications with PFC Charging Function," 2019 22nd International Conference on Electrical Machines and Systems (ICEMS), Harbin, China, 2019, pp. 1-5.

[8]. H.-C. Chang and C. -M. Liaw, "An Integrated Driving/Charging Switched Reluctance Motor Drive Using Three-Phase Power Module," in IEEE Transactions on Industrial Electronics, vol. 58, no. 5, pp. 1763-1775, May 2011.

[9]. H. Cheng, Z. Wang, S. Yang, J. Huang and X. Ge, "An Integrated SRM Powertrain Topology for Plug-In Hybrid Electric Vehicles With Multiple Driving and Onboard Charging Capabilities," in IEEE Transactions on Transportation Electrification, vol. 6, no. 2, pp. 578-591, June 2020.

[10]. H. -C. Chen and B. -W. Huang, "Integrated G2V/V2G Switched Reluctance Motor Drive With Sensing Only Switch-Bus Current," in IEEE Transactions on Power Electronics, vol. 36, no. 8, pp. 9372-9381, Aug. 2021.

[11]. J. Cai and X. Zhao, "An On-Board Charger Integrated Power Converter for EV Switched Reluctance Motor Drives," in IEEE Transactions on Industrial Electronics, vol. 68, no. 5, pp. 3683-3692, May 2021.

[12]. F. Meng, Z. Yu, Y. Chen, C. Gan and R. Qu, "Development of Switched Reluctance Motor Drives with Power Factor Correction Charging Function for Electric Vehicle Application," 2019 22nd International Conference on Electrical Machines and Systems (ICEMS), Harbin, China, 2019, pp. 1-6.